AGU PUBLICATIONS

Geophysical Research Letters

RESEARCH LETTER
10.1002/2015GL065459

Key Points:
- Crustal viscosity estimates are most similar to predictions for an andesitic lower continental crust
- The andesitic model predicts aggregate viscosities similar to feldspar
- An andesitic crust is ~1 order of magnitude less viscous than basaltic crust

Supporting Information:
- Supporting Information S1
- Figure S1
- Figure S2

Correspondence to:
W. J. Shinevar,
shinevar@mit.edu

Citation:
Shinevar, W. J., M. D. Behn, and G. Hirth (2015), Compositional dependence of lower crustal viscosity, *Geophys. Res. Lett.*, *42*, 8333–8340, doi:10.1002/2015GL065459.

Received 20 JUL 2015
Accepted 25 SEP 2015
Accepted article online 30 SEP 2015
Published online 23 OCT 2015

Compositional dependence of lower crustal viscosity

William J. Shinevar[1,2], Mark D. Behn[3], and Greg Hirth[1]

[1]Department of Earth, Environmental, and Planetary Sciences, Brown University, Providence, Rhode Island, USA, [2]Massachusetts Institute of Technology/Woods Hole Oceanographic Institution, Joint Program in Oceanography/Applied Ocean Science and Engineering, Woods Hole, Massachusetts, USA, [3]Department of Geology and Geophysics, Woods Hole Oceanographic Institution, Woods Hole, Massachusetts, USA

Abstract We calculate the viscosity structure of the lower continental crust as a function of its bulk composition using multiphase mixing theory. We use the Gibbs free-energy minimization routine Perple_X to calculate mineral assemblages for different crustal compositions under pressure and temperature conditions appropriate for the lower continental crust. The effective aggregate viscosities are then calculated using a rheologic mixing model and flow laws for the major crust-forming minerals. We investigate the viscosity of two lower crustal compositions: (i) basaltic (53 wt % SiO_2) and (ii) andesitic (64 wt % SiO_2). The andesitic model predicts aggregate viscosities similar to feldspar and approximately 1 order of magnitude greater than that of wet quartz. The viscosity range calculated for the andesitic crustal composition (particularly when hydrous phases are stable) is most similar to independent estimates of lower crust viscosity in actively deforming regions based on postglacial isostatic rebound, postseismic relaxation, and paleolake shoreline deflection.

1. Introduction

The viscosity structure of the middle and lower continental crustal plays an important role in controlling many tectonic processes including postseismic stress evolution [*Freed*, 2005], lower crustal flow [*Clark et al*., 2005], and decompression melting due to postglacial isostatic rebound [*Jull and McKenzie*, 1996]. Estimates of crustal viscosity are typically constrained by either direct analyses of postglacial rebound, postseismic relaxation, and paleolake shoreline deflection [*Thatcher and Pollitz*, 2008; *England et al*., 2013; *Shi et al*., 2015] or indirect estimates based on laboratory-derived flow laws for crust-forming rocks and minerals. The viscosity of the crust depends strongly on the mineral phases present and therefore is controlled by the bulk composition of the lower crust. Here we define the lower crust as $>$15 km depth, corresponding to the portion of the crust where deformation is dominated by viscous processes.

While the composition of the upper continental crust can be determined relatively precisely by direct sampling, the composition of the lower crust has proven more difficult to estimate [e.g., *Hacker et al*., 2015]. Because relatively few lower crustal rocks outcrop at the surface, compositional estimates for the lower continental crust typically rely on proxy measurements, such as seismic wave speeds and heat flow [e.g., *Holbrook et al*., 1992; *Christensen and Mooney*, 1995; *Rudnick and Fountain*, 1995; *Huang et al*., 2013]. Unfortunately, these proxies place relatively weak constraints on crustal composition [*Behn and Kelemen*, 2003] with compositional estimates for the lower crust ranging from basaltic [*Rudnick and Gao*, 2003] to andesitic [*Hacker et al*., 2011, 2015]. The wide range of permissible compositions has led to different models for the formation and evolution of the continental crust [e.g., *Hacker et al*., 2015].

In this study, we evaluate the compositional dependence of crustal viscosity using multiphase mixing theory for different end-member lower crustal compositions (e.g., basaltic versus andesitic). For a given composition, we use thermodynamic phase equilibria calculations to estimate the stable mineral assemblage present under pressure and temperature (P-T) conditions appropriate for the lower crust. Based on laboratory-derived flow laws for the different crust-forming minerals, we then use mixing theory to calculate the bulk viscosity of the lower crust. Finally, we compare our predictions to independent geodetic estimates of lower crustal viscosity in actively deforming regions and show that the calculated viscosities are most consistent with an andesitic lower crust.

Table 1. End-Member Crustal Compositions

Oxide	Basaltic [*Rudnick and Gao*, 2003]	Andesitic [*Hacker et al.*, 2011]
SiO_2	53.4	64.4
TiO_2	0.8	0.7
Al_2O_3	16.9	14.8
FeO[a]	8.6	6.1
MgO	7.2	2.5
CaO	9.6	3.4
Na_2O	2.7	2.8
K_2O	0.6	1.5
Total	99.8	99.6

[a]Combined wt % of ferrous and ferric iron.

2. Methods

In most previous studies in which laboratory data are used to estimate crustal viscosity, the rheology of the lower continental crust is assumed to be characterized by a single dominant mineral phase (e.g., quartz or feldspar). However, the lower crust is composed of multiple mineral phases, with abundances that are controlled by the bulk composition and the in situ pressure and temperature conditions. Here we investigate two end-member estimates for the composition of the lower continental crust (Table 1). The first is a basaltic end-member based on *Rudnick and Gao* [2003], which contains 53.4 wt % SiO_2; the second is an andesitic end-member proposed by *Hacker et al.* [2011] with 64.4 wt % SiO_2.

To calculate the equilibrium mineral assemblage for each end-member crustal compositions, we use the Gibbs free-energy minimization routine Perple_X [*Connolly*, 2009]. In our calculations, we assume a minimum equilibrium temperature of 500°C. Pressure and temperature (P-T) conditions in the crust are taken from typical continental geotherms for actively deforming regions (~80 mW/m^2) [*Lee and Uyeda*, 1965; *Pollack and Chapman*, 1977]. The lower continental crust typically contains 0–1 wt % H_2O [*Huang et al.*, 2013]. As a first-order model we calculate anhydrous mineral assemblages and incorporate the influence of H_2O solely through its effect on the viscosity of nominally anhydrous mineral phases (section 3). The role of hydrous phases (e.g., amphibole and mica) on crustal viscosity is then discussed in section 4. For all Perple_X calculations, we assume that 25 mol % of the total iron oxide is ferric [*Cottrell and Kelley*, 2011; *Kelley and Cottrell*, 2012]; variations in this value have little influence on our final crustal viscosity estimates. Solution models for crustal minerals are taken from *Hacker* [2008].

To calculate crustal viscosity from the equilibrium mineral assemblages, we employ mixing theory to determine the aggregate viscosity for different crustal compositions as a function of depth along an assumed geotherm. Theoretical and experimental investigations of rocks show that strain rate and stress fit a power law relation of the form

$$\dot{\varepsilon} = A f_{H_2O}^{r} \sigma^{n} \exp\left(-\frac{Q + PV}{RT}\right) \quad (1)$$

where $\dot{\varepsilon}$ is the strain rate, A is a preexponential constant, f_{H_2O} is the water fugacity, r is the fugacity exponent, σ is the stress, n is the stress exponent, Q is the activation energy, P is the pressure, V is the activation volume, R is the gas constant, and T is the temperature.

To include the effects of pressure and temperature on water fugacity into equation (1), we fit the thermodynamic database of *Pitzer and Sterner* [1994] (using Withers' fugacity calculator, http://www.geo.umn.edu/people/researchers/withe012/fugacity.htm) into a single equation appropriate for a range of crustal geotherms using an equation of the form

$$f_{H_2O} = a_{H_2O} A_1 \exp\left(-\frac{A_2 + PA_3}{RT}\right) \quad (2)$$

where a_{H_2O} is the water activity and A_1, A_2, and A_3 are empirically fit constants. Unless otherwise noted a_{H_2O}. Equation (2) is fit simultaneously with fugacities at P and T values along 60, 80, and 100 mW/m^2 geotherms (supporting information Figure S1), resulting in values of 5521 MPa, 31.28 kJ/mol, and -2.009×10^{-5} m^3 for A_1, A_2, and A_3 ($R^2 = 0.9996$).

The viscosities of different crust-forming minerals vary greatly (Figure 1). Based on our phase equilibria calculations (Figure 2), we consider four major crustal minerals: quartz, feldspar (plagioclase + alkali feldspar), pyroxene (orthopyroxene + clinopyroxene), and garnet, which typically make up >90% of the crust by volume in our anhydrous calculations. Flow law coefficients for quartz, feldspar, and pyroxene are taken directly from *Hirth et al.* [2001], *Rybacki et al.* [2006], and *Dimanov and Dresen* [2005], respectively. The pyroxene flow law is

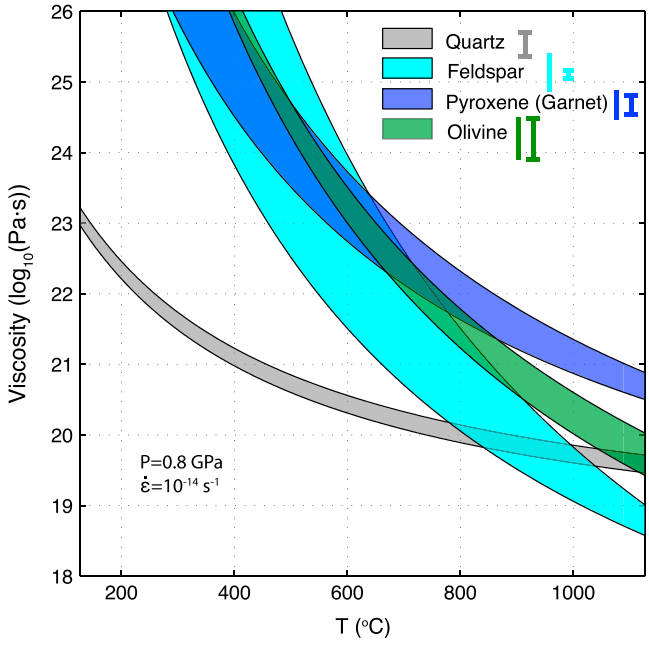

Figure 1. Viscosity as a function of temperature for major crust-forming minerals. Upper and lower viscosity bounds are calculated under dry and wet conditions, respectively. Specifically, bounds are calculated for quartz ($a_{H_2O} = 0.1$, $a_{H_2O} = 1$) [*Hirth et al.*, 2001], plagioclase (dry, wet) [*Rybacki et al.*, 2006], and pyroxene (dry, wet) [*Dimanov and Dresen*, 2005]. Note that garnet is assumed to follow the same flow law as pyroxene (see text for discussion). Olivine (dry, wet) [*Hirth and Kohlstedt*, 2003] is shown for comparison. In this study, only wet quartz is assumed to undergo dislocation creep. Viscosity error bars (denoted by small bars in the legend) are calculated at 600°C and 0.8 GPa and are shown to scale for each flow law. The bars without lines are for dry flow laws (upper bound) and the bars with lines are for wet flow laws (lower bound).

modified by introducing a linear water fugacity term, in which the published preexponential coefficient is recalculated accordingly ($A = A_{experimental}/f_{H_2O}$ for the experimental fugacity).

Intriguingly, all available garnet flow laws predict effective viscosities lower than plagioclase at crustal conditions (supporting information Figure S2). However, analyses of naturally deformed garnet-rich rocks clearly illustrate that garnet is stronger than plagioclase at crustal conditions [e.g., *Ji and Martignole*, 1994]. This suggests that the garnet laws derived under wet conditions at high temperature and pressure do not extrapolate well to lower crustal conditions. We therefore assume that the garnet flow law can be approximated by the pyroxene law, which is 1–2 orders of magnitude stronger than that of plagioclase and is the strongest flow law in our models (Figure 1).

Using the mineral proportions calculated from Perple_X, we use the mixing model of *Huet et al.* [2014] to calculate aggregate viscosity of the mineral assemblage assuming deformation occurs via dislocation creep of all phases. *Huet et al.* [2014] defines the effective aggregate viscosity as

$$\eta_{aggregate} = \sum_i \frac{\phi_i n_i}{n_i + 1} \prod_i \left(\eta_i \frac{n_i + 1}{n_i} \right)^{\frac{\phi_i a_i n_i}{\sum_i \phi_j a_j n_j}} \quad (3)$$

where ϕ_i and n_i are the volume percentage and stress exponent of phase i, respectively, and the parameter a is defined for each phase as $a_i = \prod_{i \neq j}(n_j + 1)$. This method assumes a large enough scale that the rock can be considered homogeneous and isotropic.

We explore viscosity calculated along continental geotherms for actively deforming regions assuming radiogenic heat production in the lower crust and surface heat flows of 80–100 mW/m^2 [*Jagoutz and Behn*, 2013] and strain rates from 10^{-11} s^{-1} to 10^{-16} s^{-1}. Depths are calculated from pressure assuming a mean crustal density of 2800 kg/m^3. We also compare our results to an effective viscosity for brittle deformation calculated using a frictional yield criterion for a strike slip fault assuming hydrostatic pore pressure [*Chen and Morgan*, 1990; *Behn et al.*, 2007].

3. Calculations of Lower Crustal Viscosity

We first calculate crustal viscosity for the two end-member compositions without the presence hydrous phases along an 80 mW/m^2 crustal geotherm, assuming a background strain rate of 10^{-14} s^{-1} (Figure 3). This strain rate is equivalent to tectonic plate displacement rates (order cm/yr) distributed over a 100 km wide zone of deformation. Under these conditions, we find that the basaltic end-member composition results in viscosities that decrease from 6.3×10^{22} to 5.0×10^{20} Pa·s over the depth interval from 15 to 40 km (Figure 3). The viscosity of the andesitic end-member is approximately 6 times lower without

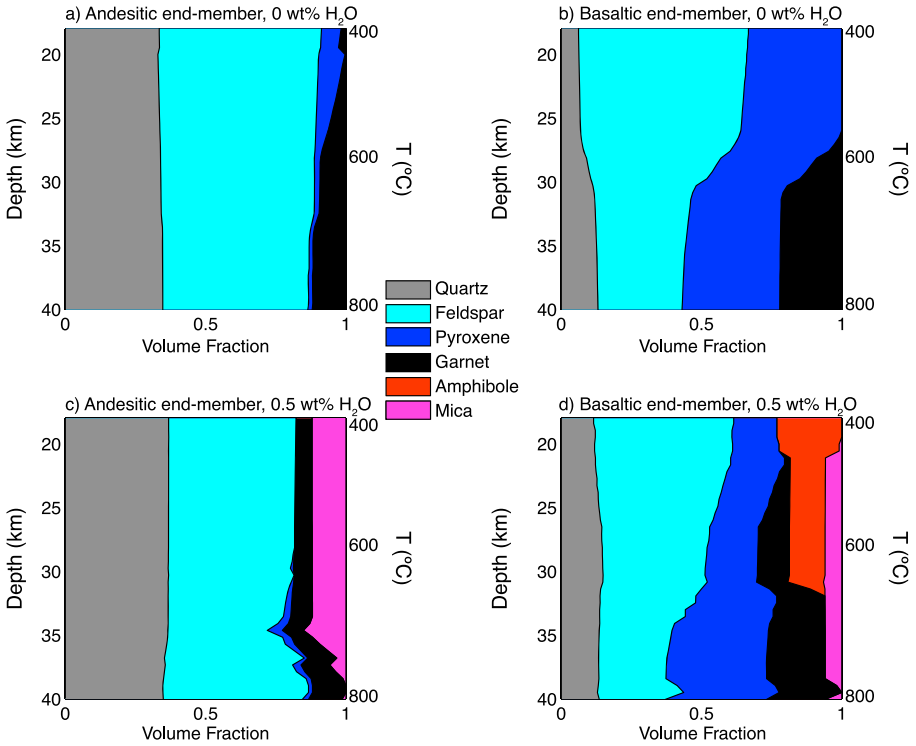

Figure 2. Mineral proportions (in volume percentage) calculated along a 80 mW/m^2 geotherm for the andesitic and basaltic end-member compositions under (a, b) anhydrous (0 wt % H_2O) and (c, d) hydrous (0.5 wt % H_2O) conditions, respectively. The addition of water does not significantly change the proportions of the mafic versus felsic mineral phases in the aggregate.

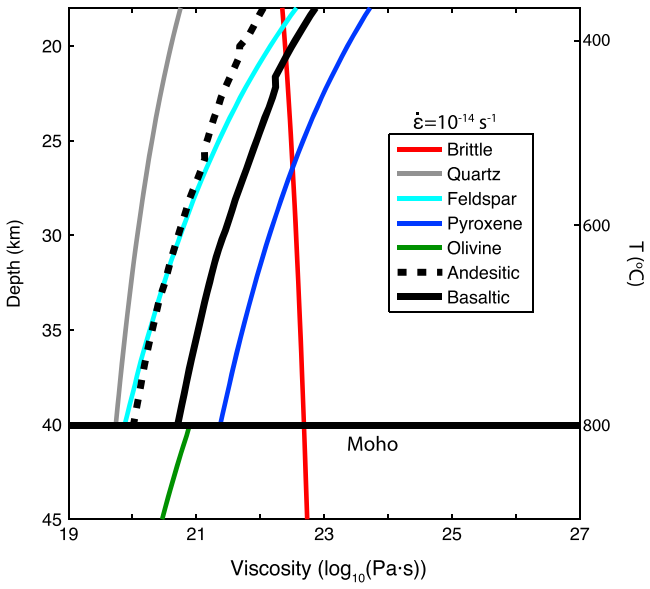

Figure 3. Viscosity versus depth calculated for the basaltic (black solid) and andesitic (black dashed) end-member crustal compositions along an 80 mW/m^2 crustal geotherm with a background strain rate of 10^{-14} s^{-1}. Shown for comparison are viscosities calculated for individual mineral phases and the effective viscosity inferred from a frictional yield criterion for a strike slip fault assuming hydrostatic pore pressure [*Behn et al.*, 2007]. The horizontal black line at 40 km depicts the Moho, below which the olivine flow law dominates.

including the effect of hydrous phases, with viscosities ranging from 10^{22} to 10^{20} Pa·s over the same depth interval (Figure 3). These differences in aggregate crustal viscosity are also manifested as a ~5 km decrease in depth to the predicted brittle ductile transition for the andesitic end-member composition.

We find that the viscosity of the andesitic end-member is similar to that of feldspar and 0.5–1.5 orders of magnitude stronger than quartz for a strain rate of 10^{-14} s^{-1} (Figure 3). By contrast, the basaltic end-member is a factor of 2–5 times stronger than feldspar and roughly an order of magnitude weaker than pyroxene. The mixing model also produces a viscosity structure that decreases less with depth compared to feldspar. This effect is caused by the increase in the proportion of stronger minerals (e.g., garnet and pyroxene) relative to quartz and feldspar with increasing depth (Figures 2a and 2b).

Along warmer crustal geotherms (100 mW/m^2) the andesitic and basaltic end-member compositions are predicted to have viscosities of 1.5×10^{19}–1×10^{21} Pa·s and 5.0×10^{19}–5.0×10^{21} Pa·s, respectively (Figure 4). Variations in strain rate also result in changes to the aggregate crustal viscosity, with an order of magnitude increase in strain rate resulting in a factor of ~6 decrease in viscosity for both end-member compositions (Figure 4c).

4. Effect of Hydrous Phases on Lower Crustal Viscosity

An important caveat to the calculations presented in section 3 is that the influence of hydrous phases is not included. The presence of water in the lower crust stabilizes minerals such as amphibole and mica. To investigate the potential effects of these hydrous phases, we calculated aggregate mineral assemblages at the same P-T conditions for systems with 0.5 wt % H_2O (Figures 2c and 2d). For the andesitic end-member the only significant change to the mineral mode is the addition of ~13 vol % mica; the relative proportions of the other minerals remains largely unchanged (Figure 2c). By contrast, the addition of water to the basaltic end-member stabilizes up to 5 vol % mica and up to 25 vol % amphibole, with the relative proportions of the mafic versus felsic phases relatively unchanged (Figure 2d). Although the bulk water content is the same for the andesitic and basaltic end-members, the volume proportions of the hydrous phases is greater in the basaltic end-member due to the lower water content of amphibole (by weight) compared to mica. The breakdown of hydrous phases at high pressure and temperature (Figures 2c and 2d) could result in the presence of melt, which is not incorporated in our calculations.

The evaluation of viscosity estimates from these hydrous mineral assemblages requires flow laws for mica and amphibole. In general, amphibole is relatively strong, with a viscosity comparable to that of pyroxene at similar pressures and temperatures [*Hacker and Christie*, 1990]. Thus, the addition of amphibole to the basaltic end-member is unlikely to lower the aggregate viscosity. The effects of including experimental data for micas are more ambiguous. Existing flow laws for biotite [e.g., *Kronenberg et al.*, 1990] indicate that biotite is stronger than wet quartz at most lower crustal conditions ($T > 400$°C) (see supporting information Figure S2). However, experiments on quartz-muscovite aggregates indicate a factor of 2 weakening with ~15 vol % mica [*Tullis and Wenk*, 1994; *Tokle et al.*, 2013]. By contrast, little weakening is observed with mica contents less than ~10 vol % due to a lack of mica interconnection. Thus, the net effect of adding mica to the andesitic end-member is to reduce its aggregate viscosity by up to a factor of 2, as shown in Figure 4a. By contrast, the addition of water to the basaltic end-member should have only a modest effect on viscosity because most of the water is bound in amphibole.

5. Discussion

Our results show that under the same pressure-temperature and strain rate conditions, an andesitic lower crust has a viscosity that is approximately a factor of 10 (without hydrous phase) to 30 (with hydrous phases) lower than a basaltic lower crust. As discussed earlier, the bulk composition of the lower continental crust remains a matter of debate. Here we compare our calculated viscosities to independent estimates of lower crustal viscosity from geodetic constraints based on postseismic relaxation, postglacial isostatic rebound, and paleolake shoreline deflection. Geodetic viscosity estimates range from 10^{19} to 10^{21} Pa·s for tectonically active regions characterized by estimated strain rates between 10^{-13} and 10^{-14} s^{-1} [*Thatcher and Pollitz*, 2008] and average heat flow of ~80 mW/m^2 [*Lee and Uyeda*, 1965; *Pollack and Chapman*, 1977]. More recent studies give similar estimates for lower crustal viscosities ranging from 3.1×10^{18} to 3.1×10^{20} [*Hammond et al.*, 2009; *Pollitz and Thatcher*, 2010; *Chang et al.*, 2013; *England et al.*, 2013; *Shi et al.*, 2015]. In all of these studies the lower crust is modeled as a single layer with constant viscosity, and thus, we take these values as an estimate of the average viscosity over the lower crust (15–30 km; grey boxes in Figure 4). The estimates from the postseismic relaxation studies must be considered lower bounds because of the short time span (<40 years) over which relaxation has been analyzed. Nonetheless, analyses of paleolake shorelines in Tibet provide lower bounds for long-term viscosities similar to those estimated from postseismic relaxation in the same region [*England et al.*, 2013; *Shi et al.*, 2015].

Our analysis indicates that for a heat flow of 80 mW/m^2 the lower crustal viscosities calculated for the andesitic end-member are most consistent with the geodetic data. The andesitic end-member is characterized by ≥80 vol % quartz + feldspar and ~13 vol % mica throughout the lower crust, resulting in viscosities that fall within the geodetic constraints. By contrast, the basaltic end-member, which contains ~50 vol% quartz + feldspar at 30 km depth, is characterized by viscosities ≥10^{21} Pa·s—above the upper end of the viscosity range favored by

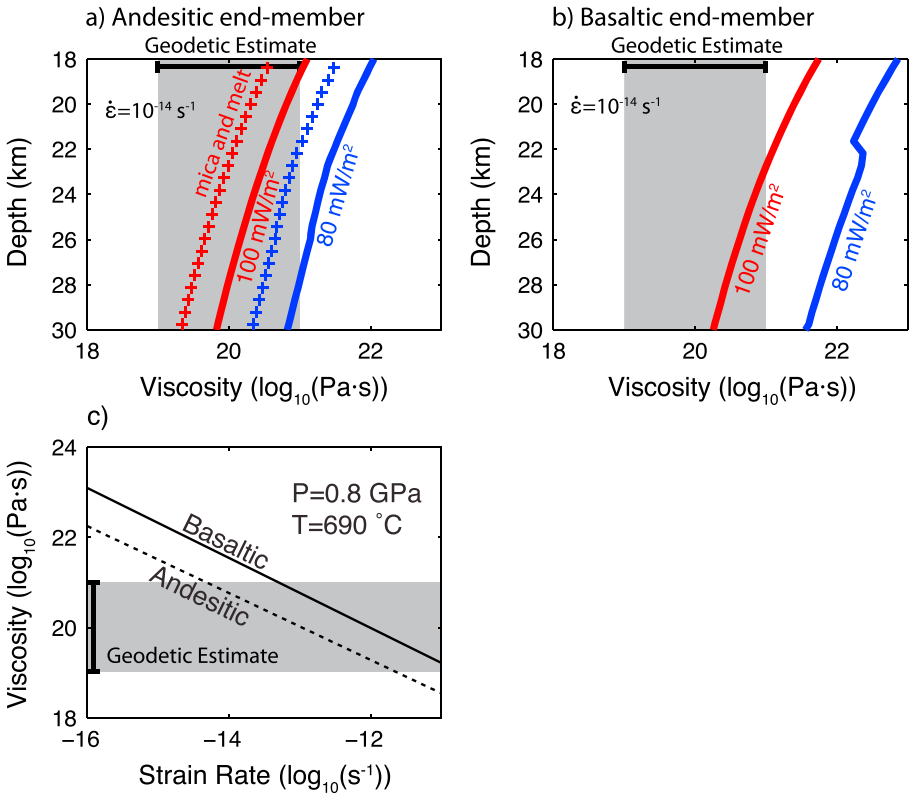

Figure 4. Viscosity calculated as a function of depth for the (a) andesitic and (b) basaltic end-member compositions along 80 mW/m^2 (blue) and 100 mW/m^2 (red) geotherms. The crossed lines in Figure 4a denote the estimated factor of 2 viscosity drop due to the presence of mica or melt (100 mW/m^2) in the modal composition. Calculations assume a background strain rate of 10^{-14} s^{-1}. Grey region denotes independent viscosity constraints from postseismic relaxation and isostatic rebound [*Thatcher and Pollitz*, 2008]. (c) Aggregate viscosity as a function of strain rate for both end-member compositions at ~30 km depth on an 80 mW/m^2 geotherm (690°C and 0.8 GPa).

the geodetic constraints. Moreover, as noted above the amount of mica present is not sufficient to dramatically decrease the aggregate viscosity of the basaltic end-member.

There are at least two additional effects on viscosity that may influence our conclusion that the andesitic end-member is most consistent with the geodetic estimates: (1) the role of strain localization and (2) the presence of melt.

Our viscosity estimates are based on a uniform crustal strain rate of 10^{-14} s^{-1}. In reality, deformation is often localized in shear zones within the lower crust [e.g., *Bürgmann and Dresen*, 2008; *Behr and Platt*, 2012] where local strain rates would be much higher. For example, if tectonic displacement rates are accommodated over a 1 km shear zone instead of a 100 km wide deforming region, the local strain rate would be ~10^{-12} s^{-1} instead of ~10^{-14} s^{-1} and the predicted viscosity for both end-member compositions decrease by more than an order of magnitude (Figure 4c). For the more rapid strain rate, the predicted viscosity for the basaltic end-member is similar to the geodetic constraints. However, the geodetic estimates of strain rate are constrained from measurements made over crustal length scales, implying that the geodetic measurements would span both regions of high strain rate, as well as intervening regions of low strain rate ($<10^{-14}$ s^{-1}). The viscosity averaged across the geodetic baseline would therefore be significantly higher than that of the individual shear zones because the geodetically determined regional strain rate is lower than the strain rate in the shear zones [cf. *Mehl and Hirth*, 2008]. Thus, viscosities calculated for high strain rate shear zones cannot be directly compared with viscosities inferred from the geodetic data.

Second, at high temperatures and pressures the breakdown of hydrous phases may lead to partial melting of the lower crust. Specifically, along the 80 mW/m^2 this occurs at depths greater than 32 and 35 for the basaltic

and andesitic end-members, respectively (Figures 2c and 2d). However, the geodetic constraints come from regions where crustal thickness is ~30 km [*Thatcher and Pollitz*, 2008]—thus, the breakdown of hydrous phases is unlikely to influence our comparison with the geodetic constraints. These effects could be more important in compressional regions (e.g., Tibet) where crustal thickness is much greater.

6. Conclusion

Our analysis of aggregate viscosities for end-member compositions of lower continental crust shows that andesitic crust is ~1 order of magnitude less viscous than basaltic crust. Further, our calculations indicate that the viscosity of the andesitic end-member is more consistent with geodetic estimates from postglacial isostatic rebound, postseismic relaxation, and paleolake shoreline deflection, particularly when hydrous phases are present. Our calculations also suggest that the aggregate viscosity of the andesitic composition (which consists of quartz, feldspar, and mafic phases) is similar to that of feldspar, justifying the use of feldspar in most geodynamic models of the lower crust.

Acknowledgments
We thank W. Thatcher, an anonymous reviewer, and Editor M. Wysession for helpful reviews that improved this manuscript. Funding for this work was provided by the Woods Hole Oceanographic Institution Summer Student Fellowship Program (W.J.S.) and NSF grants EAR-13-16333 (M.D.B.) and EAR-1220075 (G.H.). Supporting data of the fugacity fit and garnet viscosity comparisons are included as two figures in an supporting information file; all other data may be obtained on request from the corresponding author.

The Editor thanks Thorsten Becker and Wayne Thatcher for their assistance in evaluating this paper.

References

Behn, M. D., and P. B. Kelemen (2003), Relationship between seismic P-wave velocity and the composition of anhydrous igneous and metaigneous rocks, *Geochem. Geophys. Geosyst.*, *4*(5), 1041, doi:10.1029/2002GC000393.

Behn, M. D., M. S. Boettcher, and G. Hirth (2007), Thermal structure of oceanic transform faults, *Geology*, *35*(4), 307–310.

Behr, W. M., and J. P. Platt (2012), Kinematic and thermal evolution during two-stage exhumation of a Mediterranean subduction complex, *Tectonics*, *31*, TC4025, doi:10.1029/2012TC003121.

Bürgmann, R., and G. Dresen (2008), Rheology of the lower crust and upper mantle: Evidence from rock mechanics, geodesy, and field observations, *Annu. Rev. Earth Planet. Sci.*, *36*(1), 531–561.

Chang, W. L., R. B. Smith, and C. M. Puskas (2013), Effects of lithospheric viscoelastic relaxation on the contemporary deformation following the 1959 M_w 7.3 Hebgen Lake, Montana, earthquake and other areas of the intermountain seismic belt, *Geochem. Geophys. Geosyst.*, *14*, 1–17, doi:10.1029/2012GC004424.

Chen, Y., and W. J. Morgan (1990), A nonlinear rheology model for mid-ocean ridge axis topography, *J. Geophys. Res.*, *95*(B11), 17,583–17,604, doi:10.1029/JB095iB11p17583.

Christensen, N. I., and W. D. Mooney (1995), Seismic velocity structure and composition of the continental crust: A global view, *J. Geophys. Res.*, *100*(B6), 9761–9788, doi:10.1029/95JB00259.

Clark, M. K., J. W. Bush, and L. H. Royden (2005), Dynamic topography produced by lower crustal flow against rheological strength heterogeneities bordering the Tibetan Plateau, *Geophys. J. Int.*, *162*(2), 575–590.

Connolly, J. A. D. (2009), The geodynamic equation of state: What and how, *Geochem. Geophys. Geosyst.*, *10*, Q10014, doi:10.1029/2009GC002540.

Cottrell, E., and K. A. Kelley (2011), The oxidation state of Fe in MORB glasses and the oxygen fugacity of the upper mantle, *Earth Planet. Sci. Lett.*, *305*, 270–282.

Dimanov, A., and G. Dresen (2005), Rheology of synthetic anorthite-diopside aggregates: Implications for ductile shear zones, *J. Geophys. Res.*, *110*, B07203, doi:10.1029/2004JB003431.

England, P. C., R. T. Walker, B. Fu, and M. A. Floyd (2013), A bound on the viscosity of the Tibetan crust from the horizontality of palaeolake shorelines, *Earth Planet. Sci. Lett.*, *375*, 44–56.

Freed, A. M. (2005), Earthquake triggering by static, dynamic, and postseismic stress transfer, *Annu. Rev. Earth Planet. Sci.*, *33*, 335–367.

Hacker, B. (2008), H_2O subduction beyond arcs, *Geochem. Geophys. Geosyst.*, *9*, Q03001, doi:10.1029/2007GC001707.

Hacker, B. R., and J. M. Christie (1990), Brittle/ductile and plastic/cataclastic transitions in experimentally deformed and metamorphosed amphibolite, in *The Brittle-Ductile Transition in Rocks*, *Geophys. Monogr. Ser.*, vol. 56, edited by A. G. Duba et al., pp. 127–147, AGU, Washington, D. C., doi:10.1029/GM056p0127.

Hacker, B. R., P. B. Kelemen, and M. D. Behn (2011), Differentiation of the continental crust by relamination, *Earth Planet. Sci. Lett.*, *307*(3), 501–516.

Hacker, B. R., P. B. Kelemen, and M. D. Behn (2015), Continental lower crust, *Annu. Rev. Earth Planet. Sci.*, *43*, 167–205, doi:10.1146/annurev-earth-050212-124117.

Hammond, W. C., C. Kreemer, and G. Blewitt (2009), Geodetic constraints on contemporary deformation in the northern Walker Lane: 3. Central Nevada seismic belt postseismic relaxation, in *Late Cenozoic Structure and Evolution of the Great Basin–Sierra Nevada Transition*, edited by J. S. Oldow and P. H. Cashman, *Geol. Soc. Am. Spec. Pap.*, *447*, pp. 33–54.

Hirth, G., and D. Kohlstedt (2003), Rheology of the upper mantle and the mantle wedge: A view from the experimentalists, in *Inside the Subduction Factory*, edited by J. Eiler, pp. 83–105, AGU, Washington, D. C., doi:10.1029/138GM06.

Hirth, G., C. Teyssier, and J. W. Dunlap (2001), An evaluation of quartzite flow laws based on comparisons between experimentally and naturally deformed rocks, *Int. J. Earth Sci.*, *90*(1), 77–87.

Holbrook, W. S., W. D. Mooney, and N. I. Christensen (1992), Seismic velocities in the lower continental crust, in *The Lower Continental Crust*, vol. 23, edited by D. M. Fountain, pp. 1–43, Elsevier, Amsterdam.

Huang, Y., V. Chubakov, F. Mantovani, R. L. Rudnic, and W. F. McDonough (2013), A reference Earth model for the heat-producing elements and associated geoneutrino flux, *Geochem. Geophys. Geosyst.*, *14*, 2003–2029, doi:10.1002/ggge.20129.

Huet, B., P. Yamato, and B. Grasemann (2014), The Minimized Power Geometric model: An analytical mixing model for calculating polyphase rock viscosities consistent with experimental data, *J. Geophys. Res. Solid Earth*, *119*, 3897–3924, doi:10.1002/2013JB010453.

Jagoutz, O., and M. D. Behn (2013), Foundering of lower island-arc crust as an explanation for the origin of the continental Moho, *Nature*, *504*(7478), 131–134.

Ji, S., and J. Martignole (1994), Ductility of garnet as an indicator of extremely high temperature deformation, *J. Struct. Geol.*, *16*(7), 985–996.

Jull, M., and D. McKenzie (1996), The effect of deglaciation on mantle melting beneath Iceland, *J. Geophys. Res.*, *101*(B10), 21,815–21,828, doi:10.1029/96JB01308.

Kelley, K. A., and E. Cottrell (2012), The influence of magmatic differentiation on the oxidation state of Fe in a basaltic arc magma, *Earth Planet. Sci. Lett.*, *329*, 109–121.

Kronenberg, A. K., S. H. Kirby, and J. Pinkston (1990), Basal slip and mechanical anisotropy of biotite, *J. Geophys. Res.*, *95*(B12), 19,257–19,278, doi:10.1029/JB095iB12p19257.

Lee, W. H., and S. Uyeda (1965), Review of heat flow data, in *Terrestrial Heat Flow*, *Geophys. Monogr. Ser.*, vol. 8, edited by W. H. K. Lee, pp. 87–190, AGU, Washington, D. C.

Mehl, L., and G. Hirth (2008), Plagioclase preferred orientation in layered mylonites: Evaluation of flow laws for the lower crust, *J. Geophys. Res.*, *113*, B05202, doi:10.1029/2007JB005075.

Pitzer, K. S., and S. M. Sterner (1994), Equations of state valid continuously from zero to extreme pressures for H_2O and CO_2, *J. Chem. Phys.*, *101*, 3111–3116.

Pollack, H. N., and D. S. Chapman (1977), On the regional variation of heat flow, geotherms, and lithospheric thickness, *Tectonophysics*, *38*(3), 279–296.

Pollitz, F. F., and W. Thatcher (2010), On the resolution of shallow mantle viscosity structure using postearthquake relaxation data: Application to the 1999 Hector Mine, California, earthquake, *J. Geophys. Res.*, *115*, B10412, doi:10.1029/2010JB007405.

Rudnick, R. L., and D. M. Fountain (1995), Nature and composition of the continental crust: A lower crustal perspective, *Rev. Geophys.*, *33*(3), 267–309, doi:10.1029/95RG01302.

Rudnick, R. L., and S. Gao (2003), Composition of the continental crust, *Treatise Geochem.*, *3*, 1–64.

Rybacki, E., M. Gottschalk, R. Wirth, and G. Dresen (2006), Influence of water fugacity and activation volume on the flow properties of fine-grained anorthite aggregates, *J. Geophys. Res.*, *111*, B03203, doi:10.1029/2005JB003663.

Shi, X., E. Kirby, K. P. Furlong, K. Meng, R. Robinson, and E. Wang (2015), Crustal strength in central Tibet determined from Holocene shoreline deflection around Siling Co, *Earth Planet. Sci. Lett.*, *423*, 145–154.

Thatcher, W., and F. F. Pollitz (2008), Temporal evolution of continental lithospheric strength in actively deforming regions, *GSA Today*, *18*(4/5), 4–11.

Tokle, L., H. Stunitz, and G. Hirth (2013), The effect of muscovite on the fabric evolution of quartz under general shear, Abstract T53A-2559 presented at 2013 Fall Meeting, AGU, San Francisco, Calif., Dec.

Tullis, J., and H. R. Wenk (1994), Effect of muscovite on the strength and lattice preferred orientations of experimentally deformed quartz aggregates, *Mater. Sci. Eng. A*, *175*(1), 209–220.

Xu, L., S. Mei, N. Dixon, Z. Jin, A. M. Suzuki, and D. L. Kohlstedt (2013), Effect of water on rheological properties of garnet at high temperatures and pressures, *Earth Planet. Sci. Lett.*, *379*, 158–165.